Title: *FSHβ* links photoperiodic signalling to seasonal reproduction in Japanese quail.

Short Title: Annual timing in birds

Authors: Gaurav Majumdar, Timothy A Liddle, Calum Stewart, Christopher J Marshall, Maureen Bain, Tyler John Stevenson*

Affiliations: Institute of Biodiversity, One Health and Veterinary Medicine University of Glasgow, Glasgow, United Kingdom.

*Corresponding author:
Tyler John Stevenson
School of Biodiversity, One Health, and Veterinary Medicine
University of Glasgow
Glasgow, United Kingdom
e. tyler.stevenson@glasgow.ac.uk
p. 01413305793

Key words: Neuroendocrine, Photoperiod, Reproduction, Circannual, Pituitary,

This manuscript includes:
Main Text
Figure 1 to 3
Supporting Information Tables S1-S10
Supporting Information Figures S1-S6

Abstract

Endogenous programs in avian reproductive seasonal life history transitions have been known for over 30 years. Attempts to identify the neural and molecular substrates of photoperiodic time measurement have, to date, focussed on blunt changes in light exposure during a restricted period of photoinducibility. Here we report mediobasal hypothalamus (MBH) and pituitary gland specific transcript expression cascades associated with photoperiod-induced seasonal life history transitions. We identified multiple waves of transcript expression that were not synchronized across brain regions. Follicle-stimulating hormone-β (FSHβ) expression increased during the simulated vernal equinox, prior to photoinduced increases in prolactin, thyrotropin-stimulating hormone-β and testicular growth. Analyses showed sustained elevated levels of daily FSHβ expression in the pituitary under conditions of the vernal, compared to autumnal equinox, short (<12L) and long (>12L) photoperiods. FSHβ expression increased in Quail held in non-stimulatory photoperiod, indicative of an endogenous programmed change in transcription. These data identify that FSHβ provides an endogenous program for the photoperiod-dependent external coincidence timing for seasonal transitions in reproduction. FSHβ may prime the pituitary for subsequent stimulation by triiodothyronine-mediated changes in tanycytes during the photoinducible phase. Overall, the data indicate a multi-cellular, multi-neural interval timing mechanism resides in the brain to control seasonal life-history transitions in birds.

Introduction

Temperate and equatorial species display endogenous cycles in physiology and behavior that serve to anticipate future seasonal environments (Gwinner, 1986; Wingfield, 2008; Helm & Stevenson, 2014). Even in the absence of seasonal fluctuations in temperature, daylength and food availability, endogenous circannual programs in migration (Gwinner and Dittami, 1990), hibernation (Pengelley and Fisher, 1957), and reproduction (Woodfill et al., 1994; Lincoln et al., 2006) are maintained with remarkable temporal precision. The anatomical and cellular basis of circannual rhythms remain poorly characterized, but current evidence indicates that, in mammals, interval timing may reside in pituitary lactotropes (Lincoln et al., 2006) or thyrotropes (Wood et al., 2020). In most long-lived species (e.g., >2 yrs.), the annual change in daylength, referred to as photoperiod, acts to entrain endogenous circannual calendar cells to time physiological state to seasons (Bradshaw and Holzapfel, 2007). However, our understanding of how the brain integrates photoperiodic cues and endogenous rhythms to define the transitions between seasonal life-history states remains elusive.

In most birds, reptiles, and amphibians, annual changes in daylength are detected by photoreceptors located in the mediobasal hypothalamus (MBH) (Perez et al., 2019). In Japanese quail (*Coturnix japonica*), days that exceed a 'critical length' that coincides with a period of photoinducibility (Follett and Sharp, 1969) trigger a molecular cascade that starts with the upregulation of thyrotropin-stimulating hormone beta subunit (*TSHβ*) in the pars tuberalis of the pituitary gland and results in gonadal maturation (Nakao et al., 2008). The current gap in our knowledge is how short days (i.e., <12hr) induce endogenous programs in gonadal growth (Follett and Sharp, 1969) and how prolonged exposure to short days sensitises the brain to respond, at a molecular level, to stimulatory long days. Previous studies in European starlings (*Sturnus vulgaris*) demonstrated that exposure to short days increased Gonadotropin-releasing hormone (*GNRH*) expression in the preoptic

area (Stevenson et al., 2009; Stevenson et al., 2012a). As both GnRH and gonadal growth increased in the absence of stimulatory long day lengths, another cellular pathway must underlie the endogenous development of reproductive physiology in birds. We theorized multiple neuroendocrine regions including the preoptic area, mediobasal hypothalamus and pituitary cells are independently involved in the timing of seasonal transitions in physiology. Specifically, we hypothesized that pituitary gonadotropes establish a state of photosensitivity to stimulatory long day photoperiods and thus act as calendar cells that provide endogenous timing of gonadal growth.

Results

To address this problem, we simulated the photoperiodic regulation of seasonal physiology of Japanese quail, using sequential changes of an autumnal decrease, followed by a vernal increase in daylength and measured testes volume, body mass and abdominal fat. As anticipated (Follett and Sharp, 1969; Robinson and Follett, 1982), light phases that exceed the critical day length (i.e., >12hr) resulted in robust gonadal growth (Fig. 1a). Increases in body mass and abdominal fat deposition were delayed until the vernal increase in day lengths reached 10hrs (10v) (Fig. 1b,c). EdgeR analyses, of MBH sequences obtained using Minion, identified 1481 transcripts were differentially expressed ($P<0.05$) (Table S2), and BioDare2.0 established 398 have rhythmic patterns (Fig. 1e; Table S3). DAVID gene ontology analyses indicated that gonadotropin-releasing hormone receptor and Wnt signalling pathways were consistently identified as the predominant cellular mechanism recruited during each photoperiodic transition (Table S2). Increased proopiomelanocortin (*POMC*) expression coincided with body mass growth and abdominal fat accumulation (Fig. 1f). Thyroid hormone catabolism enzyme deiodinase type-3 (*DIO3*) increased after prolonged exposure to non-stimulatory photoperiods and was only therefore transiently elevated from 8L to 10v (10v; Fig. 1g). Highest levels of vimentin immunoreactivity in the median eminence coincided with the peak in *DIO3* expression (Fig.

108 1h) suggesting the localized removal of active thyroid hormone is limited to a short phase
109 and occurred prior to stimulatory photoperiods (Fig. 1i). The photoperiod-induced change
110 in vimentin was anatomically localized to the median eminence, as the area of
111 immunoreactivity in the dorsal 3rdV ependymal layer did not change with seasonal
112 transitions in reproduction (Fig. S1). Next, we used MinION to sequence transcripts in the
113 pituitary gland across the seasonal transitions in reproduction. EdgeR analyses identified
114 3090 transcripts were differentially expressed in the pituitary gland (Table S1). DAVID
115 gene ontology analyses identified that gonadotropin-releasing hormone receptor and
116 epidermal growth factor pathways are consistently observed across photoperiodic
117 transitions (Table S4). BioDare2.0 established that 130 transcripts were rhythmically
118 expressed (Fig. 1j; Table S5). A remarkable 96.5% (384/398) of MBH transcripts show a
119 photoperiod-induced spiked patterned and only 12/14 remaining transcripts displayed sine
120 waveforms. Conversely, 100% of pituitary transcripts conformed to sine (124/130) or
121 cosine (6/130) waveforms. The predominant rhythmic patterns of expression likely reflect
122 endogenous long-term molecular programs, characteristic of calendar cell function. *GNRH*
123 expression in the preoptic area was temporarily decreased during the 8L short photoperiod
124 indicating another nucleus specific cellular timer is present in this brain region (Fig. S1).
125 Overall, the pituitary showed a distinct transcriptomic profile compared to the MBH
126 suggesting independence in the representation of seasonal photoperiodic timing. The
127 vernal photoperiodic transition from 8L to 12v resulted in a significant increase in *FSHβ*
128 (Fig. 1k) without a change in tanycyte restructuring (Fig. 1h). Subsequent transition to 14v
129 and then 16v resulted in the upregulation of prolactin (*PRL*) (Fig. 1l) and thyrotropin-
130 stimulating hormone-β (*TSHβ*), respectively (Fig. 1m). These data establish that multiple
131 cells in the pituitary code seasonal photoperiodic time and *FSHβ* shows an endogenous
132 increase in expression prior to reproductively stimulatory photoperiods.

133 To ascertain common molecular mechanisms involved in the transcriptional
134 regulation of photoperiodically regulated transcripts, transcription factor enrichment
135 analysis was conducted on significant MBH (Table S6) and pituitary gland (Table S7)
136 transcripts. Association plots show no overlap in DNA binding motifs between MBH and
137 pituitary transcripts (Fig. S2) suggesting tissue-specific transcription binding factor
138 regulation. Within the pituitary gland, several common transcription factors, such as the
139 Jun proto-oncogene, Spi1 proto-oncogene and myocyte enhancer factor 2 (*MEF2a*) might
140 be actively involved in the photoperiodic regulation of transcript expression. These findings
141 indicate multiple transcription factors are likely recruited to control tissue-specific, and cell-
142 specific transcript expression and seasonal life history transitions in physiology.

143 To establish whether increased pituitary *FSHβ* during the vernal 12hr transition
144 reflects constitutively elevated expression or is driven by the sampling 'time of day', we
145 collected tissue samples every 3 hours from quail that transitioned to the autumnal
146 equinox (i.e., 12a), the short photoperiod (8L), vernal equinox (12v) and long photoperiod
147 (16L) seasonal phases (Fig. 2a). Photoinduced changes in testes volume confirmed
148 seasonal reproductive condition (Fig. 2b). Circadian clock genes aryl hydrocarbon receptor
149 nuclear translocator like (*ARNTL1*) and period 3 (*PER3*) exhibit robust anti-phase daily
150 waveforms in expression, in the pituitary gland (Fig. 2c,d) (Table S8). Only *ARNTL1*, but
151 not *PER3* nor *DIO2*, had a rhythmic waveform in the MBH (Table S8; Fig. S3). Consistent
152 with the previous study, *FSHβ* expression was higher at the vernal equinox compared to
153 all other photoperiod groups (Fig. 2e). *PRL* expression was higher in long photoperiod
154 (16L) compared to the two equinox and short photoperiod (8L) (Fig. 2f). *FSHβ* did not
155 display a daily rhythm (Table S8), which is likely due to the absence of D-box and E-box
156 motifs in the *FSHβ* promoter (Fig. 2g). *FSHβ* promoter does contain many DNA motifs that
157 are targeted by several transcription factors that are responsive to hormonal and nutrient
158 pathways indicating multiple upstream regulators are recruited to drive transcription. These

159 data support the conjecture that a long- term programmed increase in *FSHβ* occurs under
160 vernal non-stimulatory photoperiod, and it is not driven by short-term daily photic cues.

161 To identify if *FSHβ* expression is driven by an endogenously programmed
162 mechanism or in response to the gradual increase in light, adult quail were exposed to the
163 8L, 10v or 12v light schedules or kept in 8L for an additional 4 weeks (8Lext). The 8Lext
164 treatment permitted confirmation whether *FSHβ* expression would increase in that
165 photoperiod, and therefore reflect an internal timing mechanism. *FSHβ* expression
166 increased 19-fold after 4 additional weeks of 8L suggesting that endogenous drivers
167 initiate transcription despite no change in daylength ($P<0.05$) (Fig. 3a). But the dominant
168 stimulator of *FSHβ* expression was the transition to 10v and 12v photoperiod, which both
169 expressed significantly increased levels compared to 8L ($P<0.001$). As Opn5 was
170 identified in the pituitary transcriptome (Table S1), we then assessed its transcript
171 expression across the photoperiod treatments. We discovered that Opn5 expression
172 patterns paralleled *FSHβ* suggesting the potential for direct light detection by Opn5 and
173 subsequent regulation of *FSHβ* expression. Based on *FSHβ* promoter analyses (Fig. 2g),
174 we examined the expression of myocyte enhancer factor 2 (*MEF2a*) expression as a
175 potential upstream regulator of *FSHβ* expression. *MEF2a* remained relatively constant
176 suggesting this transcription factor binding protein is not the primary driver of *FSHβ*
177 expression (Fig. S4). Similarly, *DNMT3a* expression did not change across photoperiod
178 treatments (Fig. S4) suggesting that epigenetic modifications (i.e., DNA methylation) may
179 not provide the endogenous programmed change leading to constitutive *FSHβ* expression.
180 The precise molecular change upstream from *FSHβ* transcription remains to be identified.
181 In the MBH, *DIO3* displayed a rapid reduction in expression after transfer to 10v and was
182 found to be significantly reduced in 12v photoperiod ($P<0.001$) (Fig. 3c). There was a
183 significant difference in MBH *DIO2* expression (Fig. S4), but this observation was driven by
184 a decrease in 8ext. Interestingly, *GNRH* in the preoptic area was found to significantly

185 increase after extended exposure to short photoperiods (Fig. 3D). These data indicate that
186 endogenous switches in *FSHβ,* and possibly *GNRH* expression, in response to short
187 photoperiods may reflect multiple independent cellular timers that establish a physiological
188 state of photosensitivity.
189

190 **Discussion**

191 The data reported herein demonstrate that that multiple independent interval timers
192 are required for the control of seasonal life-history transitions in reproductive physiology
193 (Fig. 3e). The two cell types primarily implicated are thyrotropes and gonadotropes. Short
194 winter days initiate a gradual increase in *FSHβ* expression in the pars distalis and maintain
195 low *TSHβ* in the pars tuberalis. As photoperiods increase there is a steady elevation in
196 *FSHβ* expression, however, the release of FSH is prevented as daylengths are below the
197 critical threshold (i.e., 12L:12D) (Gwinner, 1986). Stimulatory daylengths longer than 12hr
198 trigger thyrotropes to increase *TSHβ* leading to a cascade of molecular events in the MBH
199 that permit GnRH to stimulate gonadotropes to release FSHβ and initiate gonadal
200 development (Nakao et al., 2008; Yoshimura et al., 2003; Yamamura et al., 2004). Note
201 that other pituitary cell types, somatotropes and corticotropes do not appear to show any
202 molecular switches across the photoperiodic phases. These findings uncover a two-
203 component mechanism for the cellular basis of the external coincidence model for the
204 avian photoperiodic response (Fig. S5). The endogenously programmed increase in *FSHβ*
205 establishes a state of photosensitivity to stimulatory day length, and *TSHβ* thryotropes in
206 the pars tuberalis monitor daylength and when light stimulation occurs during a period of
207 photoinducibility, initiate gonadal development. The two-component model is exciting as it
208 accommodates evidence for endogenous growth of quail gonads in the absence of
209 photostimulation (Follett and Sharp, 1969). Moreover, a TSH-independent programmed

210 change in *FSHβ* expression addresses how seasonal rhythms in tropical, non-photoperiod
211 birds can be regulated (Gwinner and Dittami, 1990).

212 The high-dimensionality and high-frequency analyses of seasonal transition in
213 physiology used in this study, also uncovered that photoperiod differentially regulates two
214 endocrine systems: reproduction and energy balance. *POMC* has well described roles in
215 the neuroendocrine regulation of food intake and body mass (Yeo and Heisler, 2012). Our
216 findings reveal that photoperiod induced seasonal transitions in reproduction and body
217 mass are not parallel. Based on these results we propose that a separate light-dependent
218 mechanism independently regulates reproduction and energy balance via the *GNRH* and
219 *POMC* neuronal systems, respectively. This has significant implications for understanding
220 species-specific seasonal transitions in life-histories. The comprehensive transcriptome
221 dataset generated in this study will facilitate ecological studies that seek to uncover the
222 molecular substrates which environmental cues, such as temperature, impact phenological
223 timing and mistiming in birds (Visser and Gienapp, 2019).

224

225 **Materials and Methods**

226 *Data and code availability statement*
227 All raw data are available in Extended data Table 1. R code used in Study 1 is freely
228 available and indicated in the methods reference list. The full R code used is available
229 upon request.
230
231 *Animals*
232 All Japanese quail were provided by Moonridge Farms, Exeter United Kingdom
233 (moonridgefarms.co.uk). Chicks were raised under constant light and constant heat lamp
234 conditions. From 5 weeks of age, birds were held in the Poultry facilities at the University
235 of Glasgow, Cochno Farm for the duration of the photoperiodic experiments. Food (50:50
236 mix of Johnston and Jeff, quail mix & Farm Gate Layers, poultry layers supplemented with
237 grit) and tap water was provided ad libitum. All procedures were in accordance with the
238 National Centre for the Replacement, Refinement and Reduction of Animals in Research
239 ARRIVE guidelines (https://www.nc3rs.org.uk/revision-arrive-guidelines). All procedures
240 were approved by the Animal Welfare and Ethics Review Board at the University of
241 Glasgow and conducted under the Home Office Project Licence PP5701950.
242
243 *Study 1 – Photoperiod-induced transition in seasonal life history states*
244 Male quail (N=108) were housed in a summer-like long-day (LD) photoperiod (16L:8D). To
245 mimic the autumnal decline and subsequent vernal increase in the annual photoperiodic

246 cycle, birds were exposure to a sequential change in day length from 16L, to 14L, to 12L,
247 to 10L, to 8L, then back to 10L, to 12L, to 14L and lastly 16L (Fig.1a). Each photoperiod
248 treatment lasted for 2 weeks to minimize the impact of photoperiodic history effects
249 (Stevenson et al., 2012a). At the end of each photoperiodic treatment a subset of quail
250 (n=12) was pseudo randomly selected for tissue collection. Birds were killed by cervical
251 dislocation followed by jugular cut. A jugular blood sample was collected in 50ul heparin
252 (Workhardt, UK) and stored at -20°C. Brain and pituitary stalk were rapidly dissected,
253 frozen on powdered dry ice and stored at -80°C. Testes were dissected and weighed to
254 the nearest 0.001g using the Sartorius microbalance (Sartorius, Germany). The length and
255 width of the testes were measured using callipers and volumes were calculated using the
256 equation for a spheroid (4/3 × 3.14 × [L/2] × [W/2]2) (King et al., 1997). Body mass was
257 measured using an Ohaus microscale to the nearest 0.1g. Fat score was assessed using
258 the common scale developed by Wingfield and Farner (1978). The scale range is 0 to 5,
259 which 0 is no visible fat and 5 is bulging fat bodies that exceed the abdominal fat pads.
260
261 *Study 2 – Daily rhythms in molecular profiles during solstices and equinoxes*
262 To investigate the daily molecular representation of summer-like and winter-like solstices
263 and the autumnal and vernal equinoxes, Japanese quail (N=188) were subjected to the
264 same photoperiodic treatments described in Study 1. A subset of quail was pseudo
265 randomly selected after the autumnal 12L:12D (n=47), short day 8L:16D (n=48), vernal
266 12L:12D (n=46) and long day 16L:8D (n=47) treatment conditions. For each of the four
267 photoperiodic treatment conditions, five-six birds were collected shortly after lights on
268 (Zeitgeber time (zt) 0), and then every three hours for twenty-four-hour period. This
269 resulted in a high frequency daily sampling period that included zt0, zt3, zt6, zt9, zt12,
270 zt15, zt18, and zt21. Brain, pituitary gland, and liver was extracted and stored at -80°C.
271 Testes mass was determined as described above.
272
273 *Study 3 – Endogenous programming of FSHβ in the quail pituitary gland*
274 Male quail (N=24) were housed in LD photoperiod for 2 days, and then day length was
275 decreased to 12hr for one day, and then 8L for six weeks. A subset of quail was killed by
276 Home Office approved Schedule 1 methods and established the photoregressed 8L group
277 (n=6). To examine endogenous increase in FSHβ expression, a subset of birds (n=6) was
278 maintained in SD photoperiods for four more weeks (8Lext). The other twelve birds were
279 transitioned to the 10L:14D (10v) light treatment for 2 weeks and another subset of birds
280 were collected (n=6). The last subset of birds was transitioned to 12L:12D (12v) for two
281 weeks and were then killed (n=6). For all birds, the brain and pituitary glands were
282 dissected and immediately frozen in dry ice and then placed at -80°C. This experimental
283 design provided the ability to examine endogenous changes in pituitary cell function via
284 the 8Lext group, and the photoinduced increase in photosensitivity (i.e., 10v and 12v).
285
286 *Hypothalamic and pituitary dissection*
287 During brain extraction the pituitary stalk was severed. The procedure leaves pituitary
288 gland components of the pars intermedia, pars distalis and pars nervosa resting in the
289 sphenoid bone. To isolate the anterior hypothalamus/preoptic area and the mediobasal
290 hypothalamus, we used a brain matrix and coordinates based on previously published
291 anatomical locations (Stevenson et al., 2012b; Nakao et al., 2008, respectively). Brains
292 were placed ventral surface in an upward direction. For the anterior hypothalamus/preoptic
293 area a 2mm diameter from 2mm brain slice was collected. The rostral edge of the optic
294 nerve was identified and then a 1mm cut in the rostral and 1mm cut in the caudal direction
295 was performed. Brain slices were checked to confirm the presence of the tractus
296 septomesencephalicus in the rostral section and the decussation supraoptica dorsalis in
297 the caudal section. These anatomical regions reliably capture the GnRH neuronal

population in birds (Stevenson and Ball, 2009). The MBH was isolated from a 2mm punch from a 3mm brain slice that spanned the decessation supraoptica dorsalis to the nervus oculomotorius (Nakao et al., 2008).

Ribonucleic acid extraction and qPCR

RNA was extracted from anterior hypothalamus/preoptic area, mediobasal hypothalamus and pituitary gland tissue using QIAGEN RNesay Plus Mini Kit (Manchester, UK). Nucleic acid concentration and 260/280/230 values were determined by spectrophotometry (Nanodrop, Thermoscientific). cDNA was synthesized from 100ng RNA using SuperScript III (Invitrogen), and samples stored at −20°C until quantitative PCR (qPCR) was performed. qPCRs were conducted using SYBR Green Real-time PCR master mix with 5ul cDNA and 10ul SYBR and primer mix. PCR primer sequences and annealing temperatures are described in Extended Data Table S10. qPCRs for mRNA expression in tissue were performed using Stratagene MX3000. qPCR conditions were an initial denature step at 95°C for 10 min. Then, 40 cycles of a denature at 95°C for 30 seconds, a primer specific annealing temperature for 30 seconds, and then an extension phase at 72°C for 30 seconds. The qPCR reaction was terminated at 95°C for one-minute. A melt curve assay was included to confirm specificity of the reactions. The efficiency and cycle thresholds for each reaction was calculated using PCR Miner (Zhao and Fernald, 2005). All samples were assessed based on the Minimum Information for Publication of Quantitative Real-Time PCR guidelines (Bustin et al., 2009).

Minion transcriptome sequencing

RNA for transcriptome sequencing was extracted using QIAGEN RNesay Plus Mini Kit (Manchester, UK). RNA concentration and 260/280/230 values were determined by Nanodrop spectrophotometer. RNA was synthesized into cDNA using Oxford Nanopore Direct cDNA Native Barcoding (SQK-DCS109 and EXP-NBD104) and followed the manufacturers protocol. A total of 6 Spot-ON Flow cells (R9 version FLO-MIN106D) were used for each tissue. A single quail was randomly selected from each treatment group so that a single Flow cell had n=9 samples giving a total of N=56 quail for mediobasal hypothalamus and pituitary stalk transcriptome sequencing. Transcriptome sequencing was conducted using MinION Mk1B (MN26760, Oxford Nanopore Technologies). Sequencing was performed by MinKNOW version 20.10.3 and Core 4.1.2. The parameters for each sequencing assay were kept to 48hrs, -180mV voltage and fast5 files saved in a single folder for downstream bioinformatic analyses.

Transcriptome Analyses

The transcriptome data analysis pipeline is outlined in Extended Data Figure S6. All bioinformatic steps were conducted using R Studio and run in a Conda environment. First, fast5 files were demultiplex and basecalled by Guppy 4.2.1. Then Porechop v0.2.4 was conducted to remove adapters from reads followed by Filtlong v0.2.0 to filter long reads with minimum 25 bases and mean q weight of 9. Transcripts were aligned to the Japanese quail reference genome and transcriptome using Minimap2 v2.17 (Li, 2018). Transcript expression levels were determined using Salmon v0.14.2 and EdgeR v3.24.3 for normalisation and differential expression (Patro et al., 2017). DAVID was conducted to identify functional pathways active during the transitions across photoperiodic states (Extended Data Table 2 and Table 4) (Dennis, 2003).

BioDare2.0 analyses of significant differentially expressed genes

To identify seasonal rhythmic expression of transcripts, we selected differentially expressed genes identified by EdgeR ($P<0.05$). Data were analysed using non-linear regression for rhythmicity using the online resource BioDare 2.0 (Zielinksi et al., 2014)

(biodare2.ed.ac.uk). The empirical JTK_CYCLE method was used for detection of rhythmicity and the classic BD2 waveform set was used for comparison testing. The type of transcript rhythmicity was confirmed as (e.g., sine/cos/arcsine) or non-rhythmic (spike) expression. Rhythmicity was determined by a Benjamini-Hochberg controlled p-value (BH corrected $p < 0.1$). Data for heatmaps were clustered using PAM clustering from the cluster package (29). Heatmaps were created using the Complexheatmaps package (Gu et al., 2016). Heat maps generated from statistically significant transcripts are presented in Fig1 and Extended Data Table 3 and Table 5.

Enrichment factor identification in promoters of differentially expressed genes

To explore potential upstream molecular pathways involved in the regulation of differentially expressed genes, we conducted a transcription factor analyses. The aim was to identify which transcription factor or factors are responsible for observed changes in gene expression and whether, if any overlap occurs across tissues. Transcription factor enrichment analysis was achieved using ChIP-X Enrichment Analysis 3 (ChEA3) (Keenan et al., 2019). We used a conservative approach and only used transcripts detected as significant by BioDare 2.0 analysis (BH corrected $p < 0.05$). Enriched transcription factors were ranked using the ENCODE database and presented in Extended Data Table 6 and Table 7.

Daily waveform analyses of transcript expression

To establish rhythmicity in daily waveform expression of MBH and pituitary transcripts, we conduct cosinor analyses (Cornelissen, 2014). 2-ΔΔ Cycling time (Ct) values obtained for the genes investigated in Study 2 were subjected to cosinor analyses based on unimodal cosinor regression [$y = A + (B\dot{c}\cos(2\pi(x - C)/24))$], where A. B, and C denote the mean level (mesor), amplitude, and acrophase of the rhythm, respectively. The significance of regression analysis determined at $p < 0.05$ was calculated using the number of samples, R2 values, and numbers of predictors (mesor, amplitude, and acrophase) (Singh et al., 2013). Data are compiled in Extended Data Table 8.

Bioinformatic analyses of FSHβ promoter

To identify potential links between transcription factors identified using bioinformatic tests, and transcriptome data, we examined binding motifs in the FSHβ promoter. The upstream promotor sequence of 3500 bp (-3500 to 0) of Japanese quail FSHβ was obtained from Ensemble (http://www.ensembl.org/index.html). This promotor sequence was analysed by CiiDER transcription binding factor (TBFs) analysis tool (Gearing et al., 2019) against JASPER core database. DNA motifs in the promoter were unique for 470 transcription binding factors. The top 80 transcription binding factors were then subjected to PANTHER gene ontology enrichment analyses (Mi et al., 2013). Several pathways were discovered and included hormone responsive, epigenetic and responsive to nutrients (Extended Data Table 9).

Immunocytochemistry and histological analyses

Snap frozen brains from experiment 1 were sectioned at 20μm using a cryostat (CM1850, Leica). The tissues sections were collected in supercharged slides (631-0108, VWR) and stored in -80c till processed for staining. We used mouse monoclonal antibody (OAAEE00561, Aviva systems) raised against the Human vimentin gene (NCBI Reference Sequence: NP_003371.2). The antibody has been shown to specifically bind with vimentin expressed in avian cells (https://www.avivasysbio.com/vim- antibody-oaee00561.html). Human and quail vimentin peptide show high similarity of 86.96% similarity. We used Goat Anti-mouse Alexa Flour488 (A11001, Invitrogen) for the secondary antibody. As negative

control procedures, we performed omission of primary antibody and omission of secondary antibody.

Immunocytochemistry was performed using the standard immunofluorescence protocol (Majumdar et al., 2015) with minor modifications. Briefly, sections (brain) in slides were first enclosed in margin using ImmEdge pen (H-4000, Vector Labs). The sections were then first post fixed in 10% neutral buffered formalin (5735, ThermoScientific) for 4 hours. After fixing, the sections were washed (3 times; 5 min each) with TBS (phosphate buffer saline with 0.2% triton). Then they were blocked in 20% Bovine serum albumin (BSA) in TBS for 1 hour at room temperature (RT). Subsequently the blocking solution was removed by pipetting and the sections were incubated with primary antibody (1:300 dilution) for 2 hours at RT and finally overnight at 4°C. The next day, sections were first washed with TBS (3 times; 5 min each) and then incubated with secondary antibody (1:200 dilution) for 2 hours at RT. Finally, the sections were again washed with TBS (3 times; 5 min each) and mounted in Fluromount-G mounting media with DAPI (004959-52, Invitrogen). The dried slides were visualized using Leica DM4000B fluorescence microscope equipped with Leica DFC310 FX camera. Leica Application Suite (LAS) software was used for image acquisition. All the images were taken at constant exposure for the FITC channel at 10X and 20X magnification.

For analysis and quantification of % area, ImageJ version 1.53j was used. For this, 20X images were first converted into greyscale images (8 bit) and a threshold applied. The threshold was determined using the triangle method on multiple randomly selected images and applied for all the images. The scale of measurement in ImageJ was then set to CM in 300pixels/cm scale. A region of interest in the median eminence and dorsal 3rdV ependymal layer was specified as 300*500 pixels (1*1.67 cm scaled units) and area fraction was measured. At least 3 images from each animal were measured and averaged for each bird. A total of 27 quail were used and distributed evenly across photoperiod treatments (n=3).

Statistical analyses and figure presentation

GLM tests were conducted to test for statistical significance. One-way ANOVA with Bonferroni correction was applied to testes mass, body mass, fat score, vimentin immunoreactivity and qPCR analyses in Study 1. Two-way ANOVAs with photoperiod and zeitgebers main effects were conducted on qPCR analyses in Study 2. One-way ANOVAs were conducted for qPCR data in Study 3. qPCR data were log-transformed if violation of normality was detected. Significance was determined at $P<0.05$. Figures were generated using AdobeIllustrator and BioRender was used to create images in panels Fig1d,n; Fig3e and Extended Data Figure 6.

Acknowledgements: The authors thank Elisabetta Tolla, Christopher Elcombe, Ana Monteiro and David Hamilton for their assistance. The authors thanks Professor Gregory Ball and Neil Evans for comments on a previous version of the paper. Funding: the work was funded by a Leverhulme Trust Research Leader to TJS.

References

Bradshaw WE, Holzapfel CM (2007) **Evolution of animal photoperiodism.** *Annual Rev. Ecol. Evol. System.* **38:**1-25.

Bustin SA, Benes V, Garson JA, Hellemans J, Huggett J, Kubista M, Mueller R, Nolan T, Pfaffl MW, Shipley GL, Vandesompele J, Wittwer CT (2009) **The MIQE guidelines: minimum information for publication of quantitative real-time PCR experiments.** *Clin. Chem.* **55**:611-622.

Cornelissen G (2014) **Cosinor-based rhythmometry.** *Theoretical Biology Medical Modelling* **11**:16.

Dennis G (2003) **DAVID: Database for Annotation, Visualization, and Integrated Discovery.** *Genome Biol* **4**:R60.

Follett BK, Sharp PJ (1969) **Circadian rhythmicity in photoperiodically induced gonadotropin release and gonadal growth in the quail.** *Nature* **223**:968-971.

Gearing LJ, Cumming HE, Chapman R, Finkel AM, Woodhouse IB, Luu K, Gould JA, Forster SC, Hertzog PJ (2019) **CiiiDER: A tool for predicting and analysing transcription factor binding sites.** *PLoS One* **14**:e0215495.

Gu Z, Eils R, Schlesner M (2016) **Complex heatmaps reveals patterns and correlations in multidimensional genomic data.** *Bioinformatics* **32**:2847-2849.

Gwinner E (1986) ***Circannual Rhythms: endogenous annual clocks in the organization of seasonal processes***. Springer-Verlag.

Gwinner E, Dittami J (1990) **Endogenous reproductive rhythms in a tropical bird.** *Science* **249**:906-908.

Helm B, Stevenson TJ (2014) **Circannual rhythms: history, present challenges, future directions.** In *Annual, lunar and tidal clocks*. pp. 203-225.

Keenan AB, Torre D, Lachmann A, Leong AK, Wojciechowicz ML, Utti V, Jagodnik KM, Kropiwnicki E, Wang Z, Ma'ayan A (2019) ChEA3: **Transcription factor enrichment analysis by orthogonal omics integration.** *Nucleic Acids Res* **47**:W212–W224.

471 King VM, Bentley GE, Follett BK (1997) **A direct comparison of photoperiodic time**
472 **measurement and the circadian system in European starlings and Japanese**
473 **quail.** *J. Biol. Rhythms* **12:**431-442.
474 Li H (2018) **Minimap2: pairwise alignment for nucleotide sequences.** *Bioinformatic*
475 **34**:3094-3100.
476 Lincoln GA, Clarke IJ, Hut RA, Hazlerigg DG (2006) **Characterizing a mammalian**
477 **circannual pacemaker.** *Science*, **314**:1941-1944.
478 Maechler M (2019) **Finding groups in data": Cluster analysis extended Rousseeuw et**
479 **al.** R package version, 2(0).
480 Majumdar G, Yadav G, Rani S, Kumar V (2015) **Bird eyes distinguish summer from**
481 **winter: Retinal response to acute photoperiod change in the night-migratory**
482 **redheaded bunting.** *J Chem Neuroanat.* **68**:55-60.
483 Mi H, Muruganujan A, Thomas PD (2013) **PANTHER in 2013: modeling the evolution of**
484 **gene function, and other gene attributes, in the context of phylogenetic trees.**
485 *Nucleic Acids Res* **41**:D377–D386.
486 Nakao N, Ono H, Yamamura T, Anraku T, Takagi T, Higashi K, Yasuo S, Katou Y,
487 Kageyama S, Uno Y, Kasukawa T, Iigo M, Sharp PJ, Iwasawa A, Suzuki Y, Sugano S,
488 Niimi T, Mizutani M, Namikawa T, Ebihara S, Ueda HR, Yoshimura T (2008)
489 **Thyrotrophin in the pars tuberalis triggers photoperiodic response.** *Nature*
490 **452**:317-322.
491 Patro R, Duggal G, Love MI, Irizarry R, Kingsford C (2017) **Salmon: fast and bias-aware**
492 **quantification of transcript expression using dual-phase inference**. *Nat. Methods.*
493 **14**:417-419.
494 Pengelley ET, Fisher KC (1957) **Onset and cessation of hibernation under constant**
495 **temperature and light in the golden-mantled ground squirrel (Citellus lateralis).**
496 *Nature* **180:**1371-1372.

497 Perez JH, Tolla E, Dunn IC, Meddle SL, Stevenson TJ (2019) **A comparative**
498 **perspective on extra-retinal photoreceptor.** *Trends Endocrinol. Metab.* **30:**39-52.
499 Robinson JE, Follett BK (1982) **Photoperiodism in Japanese quail: the termination of**
500 **seasonal breeding by photorefractoriness.** *Proc R Soc B.* **215**:95-116.
501 Singh D, Rani S, Kumar V (2013) **Daily expression of six clock genes in central and**
502 **peripheral tissues of a night-migratory songbird: evidence for tissue-specific**
503 **circadian timing.** *Chronobiol Int.* **30**:1208-17.
504 Stevenson TJ, Ball GF (2009) **Anatomical localization of the effects of reproductive**
505 **state, castration, and social milieu on cells immunoreactive for gonadotropin-**
506 **releasing hormone 1 in male European starlings.** *J Comp. Neurol.* **517**:146-155.
507 Stevenson TJ, Lynch KS, Lamba P, Ball GF, Bernard DJ (2009) **Cloning of**
508 **gonadotropin-releasing hormone I complementary DNAs in songbirds facilitates**
509 **dissection of mechanisms mediating seasonal changes in reproduction.**
510 *Endocrinol.* **150**:1826-1833.
511 Stevenson TJ, Hahn TP, Ball GF (2012a) **Variation in gonadotrophin-releasing**
512 **hormone-1 gene expression in the preoptic area predicts transitions in seasonal**
513 **reproductive state.** *J. Neuroendocrinol.* **24**:267-274.
514 Stevenson TJ, Replogle K, Drnevisch J, Clayton DF, Ball GF (2012b) **High throughput**
515 **analysis reveals dissociable gene expression profiles in two independent**
516 **neuronal systems involved in the regulation of social behavior.** *BMC Neurosci.*
517 **13**:126.
518 Visser ME, Gienapp P (2019) **Evolutionary and demographic consequences of**
519 **phenological mismatches.** *Nature Ecol Evol.* **3**:879-885.
520 Wingfield JC, Farner DS (1978) **The endocrinology of a naturally breeding population**
521 **of the white-crowned sparrow (Zonotrichia leucophyrs gambelii).** *Physiol. Zool.*
522 **51**:188-205.

523 Wingfield JC (2008) **Organization of vertebrate annual cycles: implications for control**
524 **mechanisms.** *Philos. Trans. R. Soc. B. Biol. Sci.* **363**:425–4.
525 Wood SH, Hindle MM, Mizoro Y, Cheng Y, Saer BRC, Miedzinska K, Christian HC, Begley
526 N, McNeilly J, McNeilly AS, Meddle SL, Burt DW, Loudon ASI (2020) **Circadian clock**
527 **mechanism driving mammalian photoperiodism.** *Nat Commun* **11**:4291.
528 Woodfill CJI, Wayne NL, Moenter SM, Karsch FJ (1994) **Photoperiodic synchronization**
529 **of a circannual reproductive rhythm in sheep: identification of season-specific**
530 **time cues.** *Biol. Reprod.* **50**:965-976.
531 Yamamura T, Hirunagi K, Ebihara S, Yoshimura T. (2004) **Seasonal morphological**
532 **changes in the neuro-glial interaction between Gonadotropin-releasing hormone**
533 **nerve terminals and glial endfeet in Japanese quail**. *Endocrinol*. **145**:4264-4267.
534 Yeo GH, Heisler LK (2012) **Unraveling the brain regulation of appetite: lessons from**
535 **genetics**. *Nat. Neurosci.* **15**:1343-1349.
536 Yoshimura T, Yasuo S, Watanabe M, Iigo M, Yamamura T, Hirunagi K, Ebihara S. (2003)
537 **Light-induced hormone conversion of T4 to T3 regulates photoperiodic response**
538 **of gonads in birds.** *Nature* **426**:178-181.
539 Zhao S, Fernald RD (2005) **Comprehensive algorithm for quantitative real-time**
540 **polymerase chain reaction.** *J. Comput. Biol.* **12**:1045-62.
541 Zielinski T, Moore AM, Troup E, Halliday KJ, Millar AJ (2014) **Strengths and Limitations**
542 **of Period Estimation Methods for Circadian Data.** *PLoS ONE* **9**:e96462.
543

Fig. 1 - Vernal increase in pituitary *FSHβ* precedes molecular switches in MBH and testes growth.

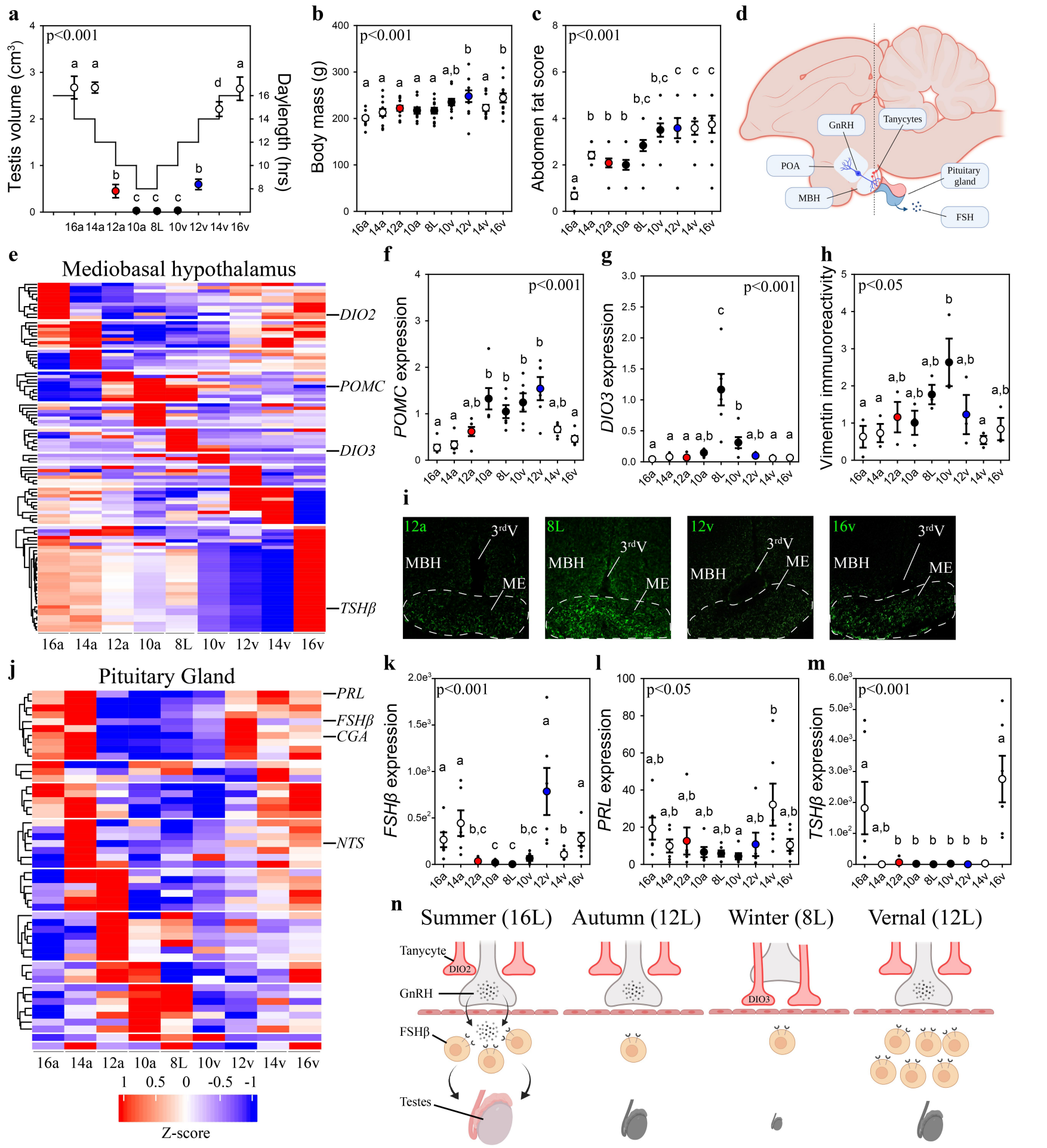

a, Schematic representation of the simulated annual rhythm in photoperiod. Quail were collected in 16hr light, 8hr dark photoperiod and then every 2 weeks the photoperiod was decreased by 2hrs to 14hr, 12hr, 10hr and then a 8L short photoperiod. Photoperiod was then increased to mimic the vernal transition and birds were collected at 10hr, 12hr, 14hr and 16hr light photoperiods. Testis volume confirmed critical day length (i.e. >12hr) induced growth. **b,** Body mass and **c,** abdomenal fat deposition increased until the autumnal equinox (12a), and then increased during the vernal photoperiod transitions. **d,** Diagram highlighting hypothalamic preoptic area (POA), mediobasal hypothalamus (MBH) and pitutiary gland. Tanycytes in the MBH gate GnRH release into the pituitary. **e,** Heat-map of RNA-seq of MBH punches identifies distinct waves of transcripts as quail transition across photoperiodic conditions. **f-g,** qPCR assays for proopiomelanocortin (*POMC*) and deiodinase type-3 (*DIO3*) confirmed restricted activation during 10v-8L and 8L-10v phases, respectively. **h-i,** vimentin immunoreactivity in the median eminence (ME) shows tanycyte morphology growth is limited to 10a, 8L, and 10v photoperiods. **j,** Heat-map illustrating photoperiodic transitions in pitutiary transcripts. **k-m,** confirmed that *FSHβ* is elevated under non-stimulatory photoperiods followed by increased prolactin (*PRL*) in 14v and thyrotropin stimulating hormone-β (*TSHβ*) in 16v. **n,** diagram summarizing that long photoperiods increase *GNRH* synthesis and release into the pituitary gland to stimulate *FSHβ* and induce testis growth. Transition to autumnal equinox phases results in reduced *FSHβ* expression and regressed testis. Prolonged exposure to short photoperiods inhibits *GNRH* expression, triggers tanycyte extension, maintains low *FSHβ* and regressed testis. Vernal transitions in photoperiod to the equinox results in resumption of *GNRH* and elevated *FSHβ* expression without testis growth. Data are mean +/- SEM, and residual dot plot. **a-c, f,g,k,m** One-way ANOVA with Bonferonni corrected Tukey's test for multiple comparisons. **h, l** One-way ANOVA with Tukey tests for significant pairwise comparison. Letters denote significant difference between photoperiod phase. Raw data available in Table S1.

Figure 2 - *FSHβ* is constitutively expressed during the vernal equinox.

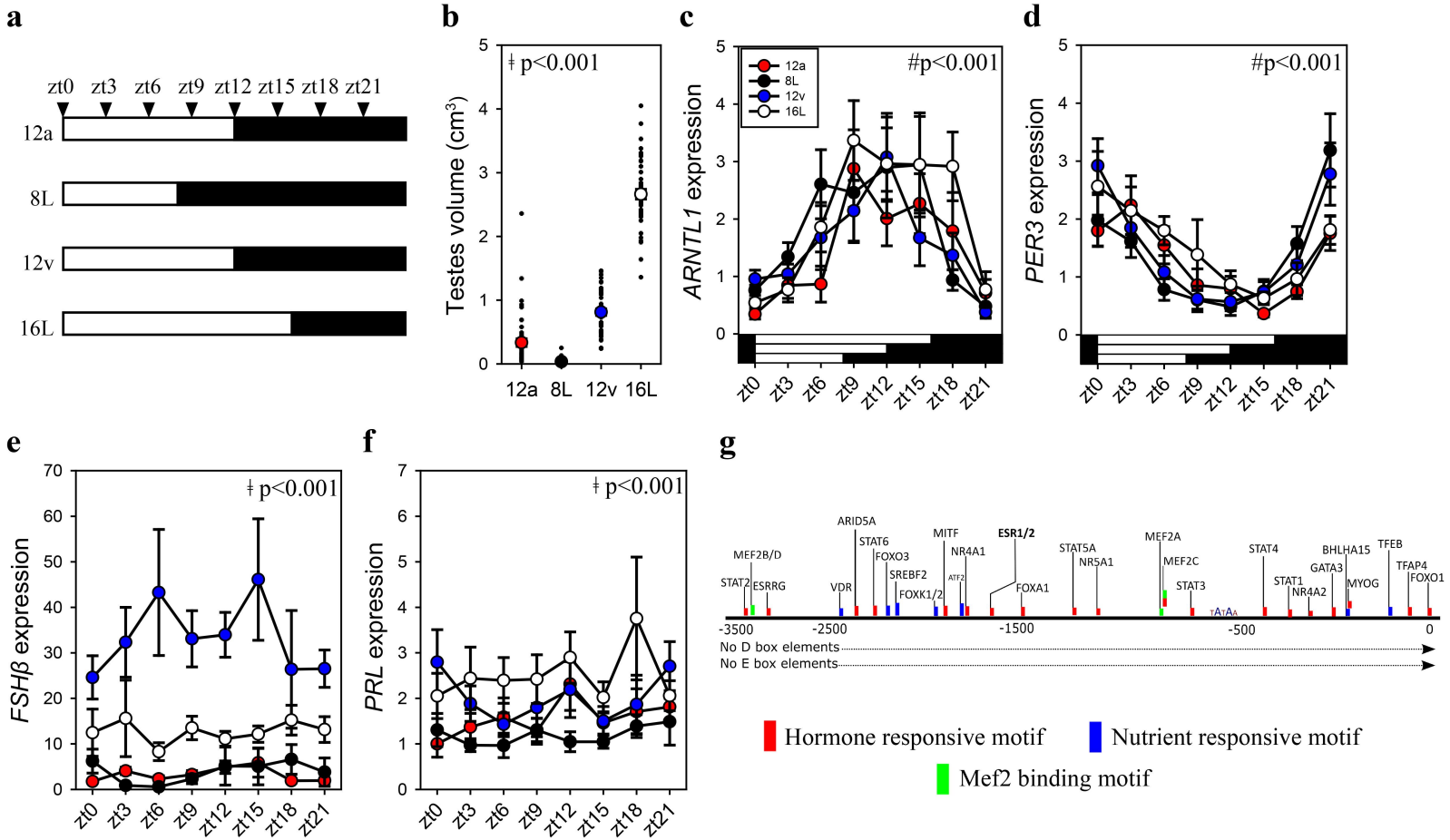

a, schematic representation of four photoperiod treatment groups with arrows to indicate the daily sampling time. **b,** testes volume remained in a regressed non-functional state in autumnal equinox (12a), short photoperiod (8L) and vernal equinox (12v). Photoperiods that exceeded the critical day length (i.e.,>12hr) induced testes growth. **c,** Pituitary circadian clock gene *ARNTL1* maintained daily rhythmic expression waveforms across all photoperiods (P<0.001) , no significant difference between photoperiod treatment (*P*=0.42) **d,** *PER3* displayed a daily waveform across 12a, 8L, 12v and 16L groups (*P*<0.001) and was anti-phase compared to *ARNTL1*. No significance difference between photoperiod treatments (*P*=0.31) **e,** *FSHβ* expression was significantly higher in 12v compared to long photoperiods (16L; *P*<0.001), autumnal equinox (12a; *P*<0.001) and short photoperiod (8L; *P*<0.001), but was not rhythmic (*P*=0.66). **f,** Similarly, *PRL* was high in 16L compared to 12a (*P*<0.001), and 8L (*P*<0.001), there was no significant daily rhythm (*P*=0.52). **g,** *FSHβ* promoter was devoid of circadian gene binding D-box and E-box motifs but contains a series of hormone and nutrient responsive motifs. **b-f** Two-way ANOVA followed by Tukey's pairwise tests, rhythmic analyses were conducted using GraphPad Prism. ǂ indicates significant photoperiod treatment effect; # denotes significant time of day effect. Data are mean +/- SEM, and residual dot plot (a-d). Rhythmic analyses are presented in Table S7 and raw data are available in Table S1.

Figure 3 - Endogenous and light-induced *FSHβ* expression.

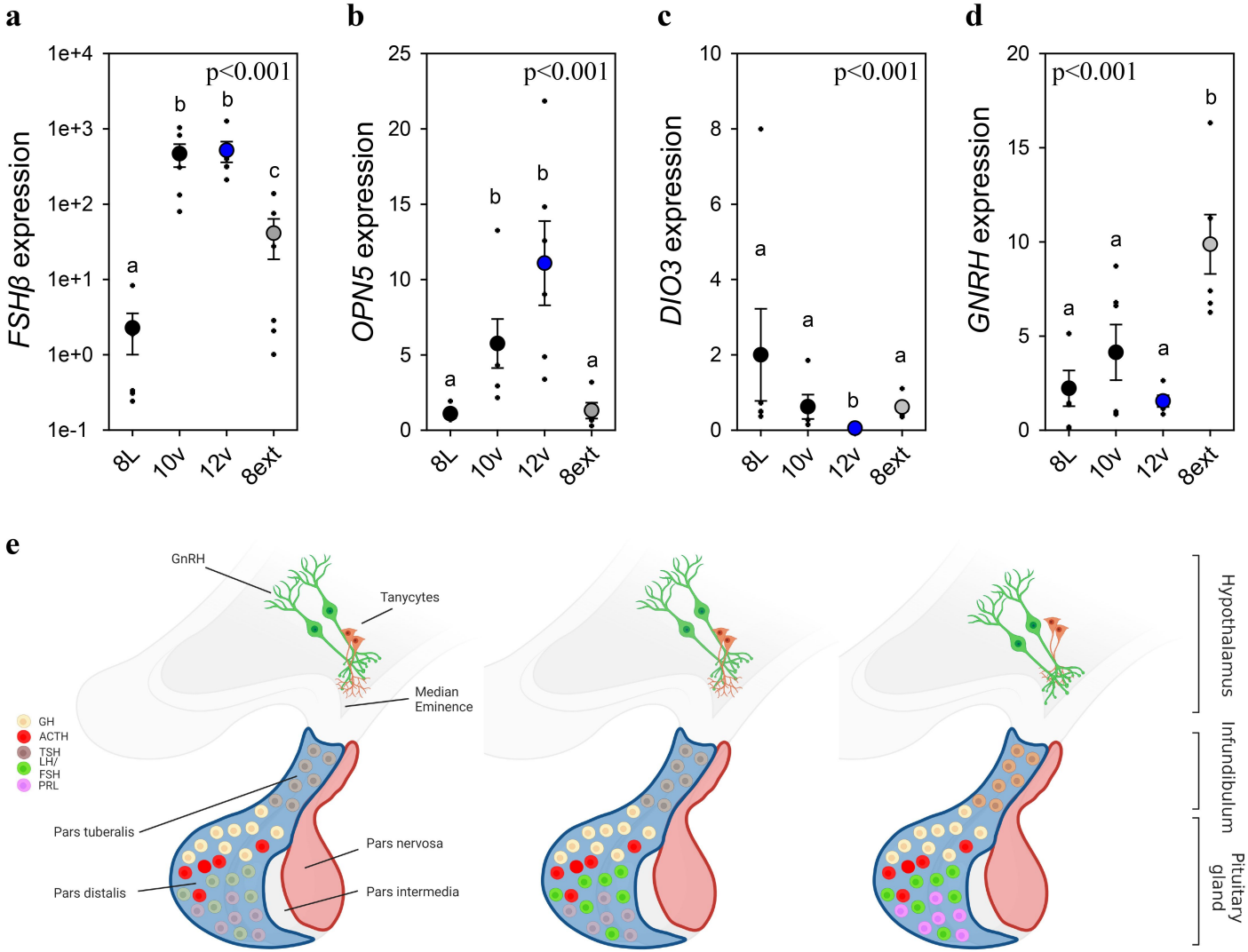

a, *FSHβ* expression increased during the photoinduced transition from 8L to 10v, and 12v. *FSHβ* also showned a smaller, yet significant increase in expression after prolonged exposure to 8L. Y-axis is presented in log-scale due to the significant increase in *FSHβ* expression in 10v and 12v. **b,** *OPN5* was detected in the pituitary gland and showed a significant increase in expression in the transition to 10v and 12v similar to *FSHβ* expression. **c,** *DIO3* was significantly reduced in 12v quail compared to all other treatment groups. **d,** *GNRH* expression remained constant during the transition from 8L to 12v. However, continued exposure to 8L was observed to increase *GNRH* expression. Data are mean +/- SEM, and residual dot plot (a-d). One-way ANOVA with Tukey's test for multiple comparisons. Letters denote significant difference between photoperiod phase. Raw data available in Table S1. **e,** Schematic representation of the endogenous and light-dependent increase in pituitary cell types during the transition from 8L to stimulatory 16v light treatments. Increased color indicates increased transcript expression.